Analysis of RNA translation with a deep learning architecture provides new insight into translation control

Xiaojuan Fan[1, 2, *, #], Tiangen Chang[4, *], Chuyun Chen[1, 3], Markus Hafner[2], Zefeng Wang[1, 3, #]

[1] Bio-med Big Data Center, CAS Key Laboratory of Computational Biology, CAS Center for Excellence in Molecular Cell Science, Shanghai Institute of Nutrition and Health,

[2] RNA Molecular Biology Laboratory, National Institute of Arthritis and Musculoskeletal and Skin Disease, Bethesda, MD, USA.

[3] University of Chinese Academy of Sciences, Chinese Academy of Sciences, Shanghai 200031, China

[4] Laboratory of Cancer Data Science, National Cancer Institute, Bethesda, MD, USA.

* These authors contributed equally to this work

[#] Corresponding to: wangzefeng@picb.an.cn, fanx3@nih.gov

Abstract

Accurate annotation of coding regions in RNAs is essential for understanding gene translation. We developed a deep neural network to directly predict and analyze translation initiation and termination sites from RNA sequences. Trained with human transcripts, our model learned hidden rules of translation control and achieved a near perfect prediction of canonical translation sites across entire human transcriptome. Surprisingly, this model revealed a new role of codon usage in regulating translation termination, which was experimentally validated. We also identified thousands of new open reading frames in mRNAs or lncRNAs, some of which were confirmed experimentally. The model trained with human mRNAs achieved high prediction accuracy of canonical translation sites in all eukaryotes and good prediction in polycistronic transcripts from prokaryotes or RNA viruses, suggesting a high degree of conservation in translation control. Collectively, we present a general and efficient deep learning model for RNA translation, generating new insights into the complexity of translation regulation.

Introduction

Computational analysis of protein-coding open reading frames (ORFs) in RNAs have traditionally relied on empirical rules such as sequence conservation pattern (1), the longest ORFs in one transcript (2) and initiation from the first AUG (3). However, these rules are over-simplified without considering the complex regulation by other factors, such as RNA structure and various regulatory *cis*-elements. As a result, previous efforts in *ab initio* prediction of translation sites achieved relatively low accuracy (4). In addition, RNA translation has recently been found in previously annotated non-coding RNAs (e.g., lncRNAs and circRNAs) (5-7), and can be initiated from alternative sites or non-canonical codons (8,9), resulting in non-annotated translation products that play critical and diverse cellular roles (6,8). Considering the complexities of translation control, the prediction of translation sites with high accuracy remains a challenging task, especially for poorly annotated genomes or in the context of complex regulatory networks. Rapid advances in artificial intelligence (AI) offer new hope for dissecting complex biological systems, such as alternative splicing (10) and protein folding (11), by uncovering hidden associations and unknown rules (12-15).

The complete synthesis of a protein requires accurate initiation and termination of translation by ribosomes at specific positions. In eukaryotes, translation initiation is generally mediated by the 5′-cap, which recruits various translation initiation factors and small ribosomal subunit to form preinitiation complex (16). This complex subsequently scans through the 5′-untranslated region (5′-UTR) to recognize the

62 optimal start codon, which is determined by both codon identity and its immediate
63 nucleotide context known as Kozak sequence GCCRCCAUGG (R represents purine)
64 (3). However, in certain cases, the ribosome may skip some weak start codons,
65 resulting in leaky scanning (3). In addition, a large fraction of genes contain several
66 alternative translation initiation sites (TISs), but it is unclear how the ribosomes select
67 one of these sites to initiate translation. Evaluating the strength of each TIS within one
68 transcript and the general rules of selecting the authentic ORFs from possible decoys
69 remain challenging. Therefore the systematic identification of translation sites
70 (translation initiation and termination sites, or TIS/TTS) and the quantitative
71 evaluation of their strength become a prerequisite for exploring the complexity of
72 translation regulation.
73 New experimental techniques, including GTI-seq (global translation initiation
74 sequencing) (17) and QTI-seq (quantitative translation initiation sequencing) (18),
75 have been developed to identify TISs by directly capturing the stalled initiating
76 ribosomes at single nucleotide resolution across the transcriptome. However, these
77 methods were typically conducted in specific cell types, which limits the
78 transcriptome-wide TIS identification. Several computational methods have also been
79 developed to predict translation initiation sites from mRNA sequences. For example, a
80 physicochemical-property based predictor using pseudo-trinucleotide composition
81 was constructed to identify TIS in human genes (19), and a variety of machine
82 learning methods have also been developed to predict the TIS by analyzing a short
83 sequence fragment (e.g. 200nt) around the start codon of mRNA (20-23). However,

such methods are biased because they are limited to the immediate sequence context surrounding the TISs. In other words, these approaches do not consider the entire non-coding regions of mRNAs (i.e. 5′-UTR and 3′-UTR) that play an important regulatory role in selecting the start codon (24,25), which in turn affects the accuracy of TIS predictions.

Here, we developed a deep learning method based on a multilevel dilated convolution network, named TranslationAI, to independently predict TISs and TTSs from full-length mRNA sequences alone. Leveraging the inherent structure of the genetic code, TranslationAI achieves high accuracy, surpassing a >99% Precision-Recall Area Under the Curve (PR-AUC) in predicting known TISs and TTSs in human transcriptome. Our model uncovered regulatory sequences in the UTRs that determine the strength of translation start and stop codons, and identified thousands of new ORFs in mRNAs or annotated lncRNAs. In addition, this model can be extended to other eukaryotes, prokaryote and several human viruses, suggesting a strong conservation in defining coding sequences across different domains of life. To facilitate further applications by other researchers, we developed a web tool (https://www.biosino.org/TranslationAI/) that is accessible to end users in predicting translation sites from RNA sequences. The application of TranslationAI extends beyond *de novo* prediction of TIS/TTS in any given transcripts, as it can also be used to evaluate the translation potential of a given RNA sequence.

Results

Modeling translation from full length mRNA with deep learning

We constructed a deep residual convolutional neural network, TranslationAI, using the full-length mRNA sequences as input to independently predict the TIS and TTS (Fig. 1A, see methods). Previous approaches only considered short sequence stretches around a potential start codon (20-22), or reported all potential ORFs in six frames with specified start codon (ATG), stop codon (TAG/TAA/TGA), and length cutoffs (ORFfinder in NCBI). In contrast, our deep learning model evaluates the potential of each position in a given mRNA to function as a TIS or TTS without using any prior knowledge of translation (e.g., the triplet or identity of genetic code). Such *ab initio* prediction enables the neural network to learn the hidden rules of translation from sequence context alone.

The deep residual neural network was constructed using the one-hot encoding of mRNA sequences as input (Fig. 1A). We built a 32-layer dilated convolution neural network architecture that produces an output matrix of the probability for the given position being a TIS, TTS or neither (Fig. S1, see methods). To obtain a comprehensive and well-curated dataset, we utilized the RefSeq gene annotation and extracted 47,098 protein-coding transcripts (47,098 TIS-TTS pairs). We trained the model using the transcripts on chromosomes 2, 4, 6, 8, 10-22, X, and Y, and tested the model with the transcripts from chromosomes 1, 3, 5, 7, and 9. The stringent top-k accuracy was used for TIS/TTS prediction. Specifically, the score cutoff was set at the point where the number of predicted sites is equal to the real number (i.e., the

127 false positive rate equal to false negative rate, the score cutoff at this point is ~0.5),
128 which ensured that only the high confidence predicted sites were considered for
129 downstream analysis.

130 To explore the effect of different input windows on test accuracy, we considered
131 four input windows that include 60, 200, 600, and 2,000 (2k) nucleotides on both
132 sides of a given position. Interestingly, the prediction accuracy improved
133 dramatically with the increasing input window size, reaching >99% PR-AUC with a
134 2k nt input window on test dataset (Fig. 1B, Table S1). Considering that >70% of
135 transcripts are longer than 2k nt (Fig. S2A), such high accuracy of TranslationAI
136 prediction is particularly remarkable, suggesting that the identity of canonical
137 TIS/TTS could be influenced by the sequences at thousands of nucleotides away,
138 potentially through long-range interactions such as RNA structure or RNA binding
139 proteins. Our findings further suggest that TranslationAI has learned to capture these
140 interactions using sequence information alone.

141 To assess the impact of sequence context on the accuracy of TIS/TTS prediction,
142 we compared the performance of the models trained on 200 and 2k nt sequence
143 context. The 2k model achieved high prediction precision (>0.95) in canonical
144 TIS/TTS prediction across a wide range of transcript lengths, however the precision
145 of the 200 nt model decreases dramatically with increase of transcript length (Fig.
146 1C). This observation is in agreement with that earlier report that distal regions far
147 away from the canonical TIS/TTS can affect the translation decision (24). With the
148 2k model, the score distribution showed a clear separation between the positive and

149 negative predictions (Fig. 1D), suggesting that the model is robust under different
150 cutoff selections. To further examine the false discovery rate (FDR), we used the 2k
151 model to score potential TISs/TTSs in the shuffled mRNA sequences. At the
152 probability score cutoff of 0.5 for both TIS and TTS, less than 5% of the ORFs in
153 shuffled dataset passed the cutoff, yielding an empirical FDR < 0.05 (Fig. 1E).
154

155 **Key features learned by the AI model for accurate prediction**

156 Encouraged by the near-perfect performance of our deep learning network in
157 predicting canonical translation sites, we sought to examine the features learned by
158 this "black box" model. We performed systematic *in silico* perturbations on different
159 regions of mRNAs to measure their effects on reducing the probability scores of the
160 authentic TISs/TTSs. Such perturbations can reflect how the AI model make the
161 accurate translation prediction in a computational sense, however a different
162 molecular mechanism may be used in cells to define translation initiation and
163 termination sites as judged by experiments. Nevertheless, it would be informative to
164 compare how a biological process like mRNA translation is perceived differently by
165 the AI model and experimental tests.

166 We found that replacing annotated TISs or TTSs with random codons
167 dramatically reduced the predicted scores of cognate sites (Fig. 1F, Table S2),
168 suggesting this model had successfully learned the identity of start and stop codons
169 from the sequence alone. Consistently, introducing a known stop codon into the
170 coding sequences (CDS) led to a drastic reduction in predicted scores of both TISs

171 and TTSs. In addition, shuffling the 5′-UTRs significantly affected the corresponding
172 TIS prediction but not TTS, whereas shuffling the 3′-UTR had little effect on
173 TIS/TTS prediction (Fig. 1G, Table S2). Notably, when both 5′-UTR and 3′-UTR
174 were simultaneously shuffled, the TIS prediction score was lower compared to the
175 cases when only the 5′-UTR was perturbed (Fig. 1G, Table S2), underscoring a
176 potential synergistic role of 5′-UTR and 3′-UTR in TIS selection. Curiously, the
177 deletions of 5′- or 3′-UTRs had less effect on TISs/TTSs prediction by this model,
178 with near perfect prediction for transcripts with only 50 nt left in the UTRs (Fig. 1G,
179 Table S2), however the underlying reason is unclear. Finally, random deletions of one
180 or two nucleotides within CDS dramatically reduced the prediction scores, whereas
181 random deletion of three nucleotides in CDS had little effect (Fig. 1H, Table S2),
182 suggesting that the model was capable of learning the triplet rule of the genetic code
183 by itself.

184 To further examine the impact of codon usage on our predictions, we introduced a
185 series of perturbations to the genetic codons of CDS. First, maintaining the same
186 amino acid compositions, the in-frame triplet shuffling or random synonymous
187 substitutions had little effect on the prediction (Fig. 1I, Table S2). We further replaced
188 codons with synonymous counterparts possessing either higher or lower Codon
189 Adaptation Index (CAI). Notably, higher CAI substitutions increased prediction
190 scores for both TIS and TTS, while lower CAI substitutions decreased these scores.
191 These findings indicate that the AI model utilizes codon choice as a crucial factor in
192 making predictions. Furthermore, we observed that nonsynonymous substitutions

193 caused a small but statistically significant reduction in prediction scores. Collectively,
194 these results suggest that the TranslationAI network has learned the intricate rules of
195 RNA translation from a subset of the transcriptome without any prior knowledge.

196 To further investigate how other sites in the full-length mRNA contributed to the
197 TranslationAI prediction, we calculated the feature importance of different positions
198 of specific transcript in predicting TIS and TTS using an occlusion sensitivity
199 analysis. Our results reveal that, while the sequences at the site of TIS and TTS
200 contribute strongly to the prediction, the other positions at different regions also have
201 various contributions (Fig. S2B). Remarkably, the importance of nucleotide at
202 different positions relative to the TIS/TTS is dependent on the specific sequence
203 contexts (i.e., the positional feature importance is different for each specific mRNA).
204 For instance, in the case of a short mRNA GPX6, we observed a great impact of TIS
205 identify on TTS prediction. In another case of a long mRNA PPP6R2, we found that a
206 position in the 5′–UTR shows high contribution to the TIS prediction. More
207 specifically, when the original sequence "TAA" is masked into "NAA" or mutated,
208 the score of the original TIS was greatly decreased (Fig. S2B).

209 In the RefSeq dataset, ~100% of the annotated ORFs follow the triplet codon rule
210 (length=3N), 98% are the longest ORFs in the transcripts, and ~40% use the first
211 AUG triplet as their start codon, raising the possibility that only using these simple
212 rules may be sufficient to make prediction. To determine the extent to which
213 TranslationAI relies on these simple rules, we generated *in silico* permutations in the
214 test dataset and measured their effects on prediction precision. The introduction of

frameshift permutations significantly reduced the prediction precision (Fig. S2C), however >50% of transcripts were still predicted to use original TIS/TTS despite breaking the 3N rule (i.e. ORF length ≠ 3N), suggesting that the rule of triplet codon is important but not mandatory for TIS/TTS prediction by TranslationAI. In addition, when ORF length was reduced by introducing premature stop codons or frameshifts, TranslationAI predicted the longest ORF in ~60% cases (Fig. S2D), again suggesting that such a simple rule was partially followed by this model. Finally, the preference for the first AUG was also affected by several permutations throughout the transcript, including changes in TIS and the introduction of early stop or frameshift (Fig. S2E). Interestingly, shortening the length of the 5′-UTR increased the ratio of first AUG usage, whereas shuffling of the 5′-UTR reduced it, suggesting that the 5′-UTR plays a critical role in TIS selection (24,25). Collectively, these results indicate that TranslationAI has learned additional features beyond simple traditional rules (i.e., the longest ORF, triplet code, and preference of the first AUG) for accurate prediction, implying that the adjacent sequences near TIS/TTS also play crucial roles in selecting translation start and stop sites.

We found no correlation (Spearman's correlation coefficient close to zero) between the predicted score of TIS/TTS and the number of transcript isoforms containing the same TIS/TTS sequences (Fig. S2F), suggesting that the scores of this model were not biased by the training data. Additionally, the TIS and TTS scores in the same ORF had a weak but statistically significant positive correlation (Spearman's correlation coefficient $r = 0.2$, $p < 1*10^{-16}$) (Fig. S2G), although they were predicted

independently. Interestingly, the TIS/TTS scores by TranslationAI showed a positive correlation with the translation efficiency estimated by the ratio of read density from Ribosome profiling (Ribo-seq) normalized by mRNA abundance (8) (Fig. S2H and S2I). This consistency aligns with previous observations (Fig. 1I), where synonymous substitutions in CDS with higher CAI exhibits higher prediction scores, while substitutions with lower CAI shows lower prediction scores. This correlation implies that that these predicted scores partially reflect their endogenous translational activities.

TranslationAI scores reveal new rule of codon selection for translation termination

We next sought to examine the hidden information of TranslationAI scores by comparing the key features between the strong and weak annotated TIS/TTS sites (the top *vs.* the bottom 5th percentile). Interestingly, the sequences surrounding strong TISs/TTSs are more conserved than those around weak TISs/TTSs (Fig. 2A), implying additional selective pressures for translation. Additionally, we examined the ribosome occupancy on the mRNAs with different TIS/TTS scores using Ribo-seq data from iPSC and iPSC-derived cardiomyocytes (8,26). Our analysis revealed that the transcripts with strong TISs or TTSs exhibit a higher ribosome peak at the start or stop positions (Fig. 2B-2C, Fig. S3A-S3B), which is consistent with their higher activity in mediating translation initiation or termination. These results suggest that the predicted scores of TISs/TTSs reflect their activities in regulating translational initiation/termination. In addition, the transcripts with weak TIS/TTS generally have a longer 5′-UTR than those with strong TIS/TTS (Fig. S3C), but such length

260 difference was observed in the 3′-UTRs only for TTS with different strengths.
261 However the implication behind such length difference is unclear.
262 We further examined the enriched sequence motifs around the strong *vs.* weak
263 TISs/TTSs (from -30 nt to +33 nt) (Fig. 2D). As expected, we found an enriched
264 motif RCCATGGC (R = A or G, with start codon underlined) at the strong TISs,
265 resembling the Kozak sequence that typically enhances translation initiation (27,28).
266 We also found a novel motif STGAG at the strong TTSs but not the weak TTSs (S =
267 C or G, with stop codon underlined, Fig. 2D). Surprisingly, the fragments
268 surrounding the strong TTS are generally biased towards CG-rich sequences,
269 implying that the C/G-rich region may mediate more efficient translation termination.
270 Moreover, the C/G enrichment showed a triplet periodicity before the strong TTSs
271 (Fig. 2D), with the third position of a codon being most C/G biased. Such codon
272 bias probably reflects the evolutionary selection under the constrain of protein
273 sequences, suggesting an unappreciated role of codon usage in translation termination.
274 To confirm this codon bias, we analyzed the 30-nt region immediately upstream
275 of the stop codon of human mRNA (equivalent of 10 codons). Consistent with the
276 motif enrichment, the synonymous codons with C/G at the third position were
277 preferably used at the upstream of strong TTSs (Fig. 2E, Fig.S3D). Remarkably,
278 such codon bias was statistically significant for all 18 amino acids with multiple
279 codons (Fig. 2E), particularly for the amino acids with 4-6 codons (e.g., Thr, Val and
280 Ser etc., Fig. S3D). Together, these results reveal an intriguing role of codon selection
281 in translation termination, and indicate that the TranslationAI has learned this codon

282 bias to make a TTS prediction.

283 To experimentally validate the unexpected role of codon bias in translation
284 termination, we designed a series of translation readthrough reporters with different
285 TTSs (Fig. 2F). This reporter contains two independent transcription units, one
286 encoding the firefly luciferase (Fluc) as a transfection control, and the other encoding
287 a fusion protein of GFP and Nano-luciferase (Nluc) separated by a set of short
288 variable sequences (45 nt) containing candidate TTSs of different strengths (Fig. 2F).
289 As a control, we inserted the sequence around the terminal codon of the human
290 vitamin D receptor (VDR) gene, which is known to undergo translation readthrough
291 (29). We further introduced different synonymous mutations before the termination
292 codon of VDR to either strengthen or weaken the TTS, and assayed the levels of
293 mRNA and translation products from these reporters (Fig. 2F and S3E). The results
294 showed that introducing the C/G-rich synonymous mutations in VDR (i.e., generating
295 a strong TTS) eliminated the product from translation readthrough (indicated by
296 arrows, Fig. 2F). Conversely, a weak TTS mutation with A/U-rich synonymous
297 codons before the stop codon increased the translation readthrough. This experiment
298 directly supported our finding on the role of codon selection in translation
299 termination. As an independent validation, we re-analyzed the Ribo-seq data from
300 two distinct cell lines to examine potential translation read through (8).

301 As expected, the ribosomal density in the 3′-UTRs following weak TTSs was
302 significantly higher than that following strong TTSs (Fig. 2G), suggesting a
303 translation “leakage” following the weak termination sites. To validate this

observation, we conducted an analysis of the ribosome profiling data, in which the cells were subjected to a high-salt wash to release vacant ribosomes lacking a nascent polypeptide(30). The results demonstrated a distinct pattern: the high-salt wash effectively released the ribosome signal at the last P-site of strong TTS, while no such release was observed at weak TTS (Fig. 2H). This specific response is consistent with above findings that ribosomes associated with weak TTS may undergo translation readthrough, allowing continued translation beyond the canonical termination site, whereas ribosomes at strong TTS are more likely to be released, terminating translation at the expected site.

Alternative TIS predicted by TranslationAI

Certain mRNAs may use alternative TIS to produce additional protein isoforms with extended N terminals (31), therefore we further examined if the TransaltionAI can predict alternative TISs that may compete with the annotated sites (see methods). Based on the distribution of TranslationAI scores (Fig. 1D), we used the score cutoff at 0.1 to increase the sensitivity of the alternative TISs prediction and identified 5336 alternative TISs in total. Interestingly, the numbers of alternative TIS identified by TranslationAI is negatively correlated with the strength of the annotated TISs in the same transcript (Fig. S3F), suggesting that alternative translation initiation may happen in the mRNA without dominant TIS. Specifically, ~55% of mRNAs with weak annotated TISs contain an alternative TIS (1340 out of 2416 mRNAs), whereas the alternative TISs were found in less than 3% of mRNAs with strong annotated TISs (68

326 out of 2352 mRNAs). In addition, the score difference between the annotated TISs and
327 the alternative TIS was much smaller in the mRNAs with weak TISs (Fig. S3G, left),
328 whereas the mRNAs with strong annotated TISs generally lack alternative TISs with a
329 competitive score (Fig. S3G, right). A consistent result was also found when we only
330 considered the alternative TISs in the same reading frame with the annotated TISs (Fig.
331 S3G). These results collectively suggested that the mRNAs with weak annotated TISs
332 may also be translated from an alternative start site.

333 Further analysis suggested that the sequences at predicted alternative TISs are less
334 conserved than the annotated TISs (Fig. S3H), suggesting that these alternative TISs
335 may be emerged more recently during evolution. The predictions of alternative TISs
336 were further supported by the Ribo-seq data obtained in two different cell lines (8),
337 where the ribosome density in the 5′-UTRs could reflect the noncanonical translation
338 initiation driven by alternative TIS. Consistently, the transcripts with a predicted
339 alternative TIS showed significantly higher ribosomal read density in their 5′-UTRs
340 compared to the mRNAs without alternative TIS (Fig. S3I), suggesting a leaky
341 translation in the UTRs due to alternative translation initiation.

342

343 **TranslationAI identifies non-canonical ORFs in human transcriptome**

344 It was recently reported that non-coding RNAs in the human transcriptome or the
345 non-coding regions of mRNAs may contain unannotated ORFs that are translated into
346 new proteins or small peptides (5,8). Therefore, we next used TranslationAI to
347 examine the noncanonical ORFs in human transcriptome. Using the stringent cutoff

348 for positive TISs/TTSs (i.e., same cutoff in mRNAs), we were able to identify 4620
349 noncanonical ORFs defined by new TIS-TTS pairs (Fig. 3A). These newly
350 predicted ORFs included 673 upstream ORFs (uORFs, exemplified in Fig. 3B), 127
351 downstream ORFs (dORFs, exemplified in Fig. 3B), 26 overlapping ORFs with
352 different reading frames from the annotated ORFs (Table S4). To validate the
353 predicted non-canonical ORFs, we compared our prediction with uORFdb that is
354 constructed from comprehensive and meticulous curation of uORF-related literature
355 (32). The analysis revealed that a remarkable 569 out of 673 (85%) uTISs were also
356 corroborated by uORFdb. In addition, 30 out of 673 (4%) uTISs were experimentally
357 supported in TISdb using ribo-seq data from HEK293 (33) (Table S4).
358 The model also identified 3794 new ORFs from annotated noncoding RNAs (Fig.
359 3A, Table S5). These results demonstrate the potential for deep learning approaches to
360 uncover previously unrecognized translation events and shed light on new regulatory
361 mechanisms in gene expression. We next validated the prediction by comparing the
362 predicted TISs in new ORFs with all TISs experimentally identified *via* ribosome
363 profiling (8). We found that TranslationAI accurately predicted 99.6% of the
364 annotated ORFs, however a smaller fraction of the noncanonical ORFs supported by
365 Ribo-seq were successfully predicted by TranslationAI (39% of uORFs, 37% of
366 dORFs, 24% of dual reading frame, and 43% new ORFs in lncRNAs were identified,
367 Fig. 3C), suggesting that this model is biased towards canonical TISs/TTSs. Since
368 the training set only contain canonical TIS/TTS information, the TranslationAI model
369 may have learned limited features of non-canonical TISs/TTSs (see discussion).

370 We further focused on the thousands of predicted new ORFs from non-coding
371 RNAs (ncRNAs), which are annotated in ENSEMBL as lncRNA, antisense RNA,
372 miRNA precursors, processed transcripts, etc. (Fig. 3D). The shuffled sequences of
373 all lncRNAs were analyzed using the same deep learning model as a background
374 control. We found that the TranslationAI indeed predicted much more ORFs in the
375 "non-coding" RNAs than their shuffled counterparts (Fig. 3E). While previous
376 reports suggested that some lncRNAs can be translated into small peptides (5-8),
377 detailed analysis of these noncanonical ORFs was inadequate. Our results showed that
378 the newly predicted ORFs in lncRNA are significantly longer (Fig. S4A) and more
379 conserved in 46 vertebrates (Fig. S4B) compared to the control ORFs defined by the
380 longest fragments between ATG and TAA/TAG/TGA in all lncRNAs, suggesting a
381 potential functionality. However, the TISs/TTSs from translatable lncRNAs have
382 lower scores and are less conserved compared to canonical TISs/TTSs from mRNAs
383 (Fig. S4C), implying that the translation efficiency of these newly identified ORFs
384 may be lower than those from annotated mRNAs. This could partially explain why
385 these 'lncRNAs' were originally defined as non-coding RNAs.
386 To validate the prediction of these new ORFs, we re-analyzed the Ribo-seq data
387 from iPSC and cardiomyocytes (8). In total 64 newly predicted ORFs by
388 TranslationAI were supported by Ribo-seq signals in either cell line (Table S5). The
389 ribosome density of translatable lncRNAs closely resembled the footprints from
390 control mRNAs, with strong trinucleotide periodicity that is indictive of active
391 translation (Fig. 3F and Fig. S4D). In addition, mass spectrometry (MS)-based

392 proteomics confirmed the stable expression of 191 non-canonical peptides (Table S5,
393 with two examples shown in Fig. 3G). Among them, the ORFs in 10 lncRNAs were
394 supported by both Ribo-seq and MS. The low number of experimentally validated
395 ORFs may be contributed by several factors, including the cell line specific
396 expression of most lncRNAs, the generally low expression level of lncRNAs, and the
397 limited recover rate in both Ribo-seq and MS experiments.
398 Notably, we have correctly predicted 10 out of the 13 translated lncRNAs
399 validated by independent functional studies, including the HOXB-AS3 that was
400 reported to encode a 53aa peptide (34), the LINC00961 that encodes a 90aa peptide
401 involved in the mTOR activation (6), and the RP11-132A1.4 that encodes a functional
402 peptide of 124aa (8). All of these three lncRNAs were mis-annotated in RefSeq,
403 probably because their expression and translation are limited to specific cell types. It
404 is also worth noted that the predicted ORFs in annotated lncRNAs generally have low
405 scores in our model (Table S5), which could be attributed to the short ORF length or
406 the presence of a long 5′-UTR. Nevertheless, these results highlight the potential
407 application of AI model in the future study of translatable lncRNA.
408
409 **TranslationAI accurately predicts TISs of other eukaryotes and viruses**
410 An "universal genetic code" is used from bacteria to mammals, suggesting that
411 translation machinery is highly conserved across different organisms. Therefore, we
412 sought to examine if the model trained on human transcriptome can also predict
413 canonical translation sites in other organisms. The accuracies of translation

414 predictions for all eukaryotes tested (Human, Mouse, Zebrafish, Drosophila,
415 Arabidopsis and budding yeast *S. cerevisiae*) were remarkably high (> 90% for all
416 predictions, except that the yeast TIS prediction accuracy is 89%, Fig. 4A), suggesting
417 that our model has learned the essential features generally required for translation
418 initiation and termination in all eukaryotes.

419 In addition, we compared TranslationAI with two existing computational models,
420 a deep learning model TITER(20) and a linear regression model TIS-predictor(23).
421 Both previous models incorporated the surrounding local sequence as input to predict
422 translation initiation sites, with TITER considering 200 nt and TIS-predictor
423 considering 23 nt on both sides of TIS. Notably, we found that TranslationAI
424 surpassed the other two models as judged by both the Area under the ROC Curve
425 (AUC) and PR-AUC of TIS prediction across all tested eukaryotes (Fig. 4A and Table
426 S1). The high performance of TranslationAI on canonical translation sites underscores
427 the significant advance of our model over the previous ones, as the new model
428 considers the entire mRNA rather than focusing solely on a limited region around
429 candidate AUGs. Additionally, while TITER and TIS-predictor were primarily
430 designed to predict non-canonical TIS by incorporating both AUG and near-cognate
431 start codons, TranslationAI was specifically developed to predict translation sites
432 without any prior bias toward non-canonical translation, and thus outperforms TITER
433 and TIS-predictor in predicting canonical TISs that account for the majority of our
434 training dataset.

435 We further assess the performance of TranslationAI model trained with human

436 transcripts on the polycistronic transcription units of E. *coli*, which may reflect how
437 much of the coding sequence might be conserved between eukaryotes and
438 prokaryotes. Surprisingly, we obtained a 65% accuracy in *E. coli* with the deep
439 learning model using all parameters trained on the human transcriptome (Fig. S5),
440 even though most *E. coli* genes are transcribed as polycistronic units with very short
441 UTRs and different set of genetic codons. Considering the lack of transcriptomic
442 and proteomic information for most bacteria, this model could be useful in predicting
443 their ORFs based solely on their genome. Furthermore, we extended this model on
444 the transcriptomes of chloroplast (from *Arabidopsis*) and mitochondrion (from
445 human), and the resulting prediction accuracies were ~30% and <1%, respectively
446 (Fig. S5). Given that the translation mechanism and the genetic codon in chloroplast
447 and mitochondrion are drastically different from the human cells, such drop of
448 prediction accuracy is not unreasonable.
449 Finally, we tested whether this model can predict the TISs/TTSs of human viruses
450 that rely on the host cell machinery for protein synthesis, albeit through different
451 translational mechanisms (35). Taking two RNA viruses (Ebola and SARS-CoV-2)
452 as examples, we found that the model trained with human data can accurately predict
453 all TISs and TTSs of Ebola virus even when we used the entire genomic RNA
454 sequence as the input (Fig. 4B and Fig. S6A). In addition to the annotated TISs and
455 TTSs, we also predicted a new internal translation start site in the GP gene in Ebola
456 (Fig. 4B), suggesting an additional translation isoform for GP with truncated N-
457 terminus.

Compared to Ebola virus, TranslationAI showed a lower prediction accuracy for SARS-CoV-2, with 8 out of 12 annotated TISs and 10 out of 12 annotated TTSs being predicted with high confidence by sub-genomic RNAs (36) (Fig. 4C and Fig. S6B). In addition, our model also made several false positive predictions of TISs/TTSs in SARS-CoV-2 genome (Fig. S6B). Similar performance was observed with either genomic or sub-genomic RNAs as input. A notable difference between these two viruses is that the Ebola genome is transcribed into monocistronic mRNAs with both UTRs, whereas the SARS-CoV-2 mRNAs are mainly polycistronic genomic or subgenomic RNAs with short spacer sequences between each ORF (36,37). This may partially explain the different performances of TranslationAI for different viruses.

Taken together, our results suggest that the model containing parameters trained on human transcriptome can accurately predict canonical ORFs in a wide range of organisms. However, in certain cases where the translation regulation is drastically different (e.g., short UTRs or different codon system), the application of this model should be carried out with caution.

Discussion

As one of the most effective and powerful machine learning methods, the deep learning network has been widely used to study complex biological questions ranging from population genetics to precision medicine (12-15). Here we developed a deep learning architecture, TranslationAI, for *ab initio* prediction and systematic analysis of translation initiation and termination in entire transcriptome. Remarkably, the model trained with ~70% of human transcripts achieved a near-perfect prediction accuracy in not only human, but also a wide range of eukaryotic organisms. The model can also identify new ORFs in annotated noncoding RNAs, some of which were confirmed by independent Ribo-seq and mass spectrometry experiments. Further analysis of this predictive model also identified a new regulation rule for translation termination, providing mechanistic insights into the complex regulation of RNA translation.

The final TranslationAI-2k model strategically utilized a flanking sequence of 1000 nt around the position of interest. We chose this design aiming to address the limitations observed in prior models that predominantly focused on characteristics of local sequences (20,23). By incorporating long-range sequence features, this model effectively captures potential interactions within mRNA sequences, including the long-range interactions of both UTRs, detecting frame shifts following one or two nucleotide deletions, and examination of codon bias within CDS.

The remarkable accuracy of TranslationAI suggests that this “black box” model have learned useful information with biological relevance. We found that the model has successfully learned the identity of canonical start and stop codons (Fig. 1F), which account for the vast majority (99.4% start codon and 99.6% stop codon) of the

498 training set. The model did not identify any TIS/TTS with noncanonical start or stop
499 (i.e, non-AUG start or non-UAG/UAA/UGA stop), probably because they are
500 extremely rare in the training data. Additional features, including triplet reading
501 frameshift, UTR sequences, and codon bias also contribute to the prediction accuracy.
502 In addition, the long-range interactions contributed to the prediction accuracy of this
503 model, as simultaneously disrupting the 5′-UTR and 3′-UTR cause synergistic effect
504 in reducing the prediction scores (Fig. 1G). Moreover, certain internal sites in each
505 mRNA also contributed to the TranslationAI prediction in a context-dependent
506 fashion (Fig. S2B), however the underlying biological mechanisms are unclear. All
507 these features contributed partially to the model in terms of TIS/TTS prediction, as
508 disrupting these features did not completely invalidate the prediction (Fig. 1G-I).
509 Surprisingly, several known features associated with translation regulation,
510 including the 3′-UTR sequence, synonymous mutation, and sequences of translation
511 product, showed small effect on the accuracy of TIS/TTS prediction, implying that
512 they may not play a dominant role in selection of translation sites. More
513 importantly, we found several new features can influence the prediction of TIS/TTS,
514 such as the G/C rich motif around the strong TTS, suggesting additional determinants
515 for translation termination. These features may open up new avenues for
516 investigating the molecular mechanisms underlying translation control. Future
517 exploration of these predictive features may provide mechanistic insights into the
518 functional interactions between the mRNA and translation machine.
519 We also used this model to assess the single nucleotide variants (SNVs) that may

520 alter the TISs/TTSs and cause functional consequences. Surprisingly, we did not
521 identify any disease-associated SNVs in the ORF that can alter the TIS/TTS
522 prediction, unless the mutation directly changed the start or stop codon. This is
523 consistent with the finding that the synonymous/non-synonymous substitutions of
524 amino acids had little effect on TIS/TTS prediction (Fig. 1I). These results suggest
525 that small changes in coding sequence do not significantly impact ORF selection by
526 the translation machinery, *i.e.,* the translation initiation and termination appear to be
527 unaffected by the elongation steps. Alternatively, it is also possible that the model
528 does not rely on the nucleotide composition within ORFs for its prediction.
529 This model also allowed us to identify novel regulatory motifs associated with
530 TIS and TTS. We discovered, for the first time, that the strong stop codons are
531 surrounded by novel motifs that are generally CG-rich, especially in the third position
532 of the codons immediately before the stop codon. Consistently, there is a codon bias
533 associated with the strong termination site (Fig. 2E), and the synonymous mutations
534 with low CG-contents will introduce translation readthrough in a reporter assay (Fig.
535 2F). Because the GC-rich codons were found to be associated with slow translation
536 (38), we speculate that the strength of the stop codon is associated with the decreased
537 translation elongation rate prior to reaching the stop codon. This regulation may be
538 attributed to the changes in the strength of ribosome's interaction with the mRNA
539 before the ribosomes reach the termination site, which “decelerate” the translation
540 before an efficient termination. Alternatively, the motif could alter the ribosome’s
541 conformation, thereby influencing translation termination. This finding suggests that

542 the translation regulation is more intricate than previously thought, and further
543 exploration on this phenomenon may shed light on the mechanism of translation
544 termination and readthrough.

545 The deep learning network trained with human transcripts achieved a surprisingly
546 high accuracy for the prediction of ORFs in bacteria, yeast, plants and certain viruses
547 using only their genome sequences as input (Fig. 4). This result is particularly
548 interesting given that some of these organisms have polycistronic transcription units
549 or genomes, suggesting that the TranslationAI can predict not only uORFs and dORFs
550 in human, but also ORFs in polycistronic sequences from other organisms. However
551 this model failed to predict mitochondrial ORFs and showed mediocre performance
552 for SARS-CoV-2, probably due to the presence of frameshift regions, overlapping
553 ORFs, and a lack of sufficient intergenic sequences to separate different ORFs.
554 These results suggest that additional training may be required to improve the model's
555 performance on more complex or noncanonical genomes.

556 Despite its high accuracy in predicting canonical TISs, TranslationAI has some
557 limitations. First, our model currently struggles in predicting non-canonical TISs,
558 especially for uTISs with non-AUG start codons. This is probably due to the bias in
559 the training dataset, which mainly consists of mono-cistronic translation units with
560 AUG start codon. We have trained the model with non-AUG TIS, however
561 distinguishing positive TISs from background proved challenging, probably due to the
562 insufficient and noise experimental data for non-AUG start codon in human
563 transcriptome. We also attempted to train this model using a subset of mRNAs with

multiple annotated ORFs, however the accuracy (~75%) was not as high as that of canonical transcripts, again possibly due to the small size of the training data. Furthermore, although this model can predict the strengths of different TISs in the presence of multiple ORFs, it is still challenging to predict which TIS will be used in specific cell lines or tissues. Expanding the ribosome profiling data in different cell types may help refine the tissue-specific translation prediction model. Finally, the model uses a stringent threshold under the assumption that there is a dominant ORF in each transcript. While this assumption holds well for most transcripts, it may be incorrect in some cases. With more non-canonical ORFs being discovered, the score threshold may need to be modified to better fit different type of transcripts. In summary, with increasing translation datasets and more refined parameters, we believe that the TranslationAI framework will improve ORF prediction and deepen our understanding of the complexity in translation control.

578 **Methods**

579 **Architecture of the TranslationAI deep learning model**

580 We constructed a deep residual neural network using one-hot encoding to
581 represent mRNA sequences as input (Fig. 1A). Our approach employed a 32-layer
582 dilated convolutional neural network architecture (Fig. S1) to generate an output
583 matrix representing the probabilities of a given position being a TIS, TTS, or neither
584 (NS).

585 Four models were developed with distinct architectures, incorporating 60, 200,
586 600, or 2,000 nucleotides on both sides of a position of interest within the full-length
587 mRNA sequence as input (Fig. S1). The segmentation of sequences into normalizing
588 input sizes (60, 200, 600, or 2,000 nt) facilitates batch processing within the
589 programming framework. Each model produces probability scores for TIS, TTS, and
590 NS, with the sum of these probabilities equaling one.

591 The TranslationAI consists of several stacked residual blocks that connect the
592 input layer to the penultimate layer, a framework previously developed for image
593 recognition (39). A convolutional unit with softmax activation links the penultimate
594 layer to the output layer. To enhance convergence speed during training, the output of
595 every fourth residual block is added to the input of the penultimate layer (Fig. S1).

596 The fundamental unit of the TranslationAI model is a residual block, which
597 contains two batch-normalization layers, two rectified linear units (ReLU), and two
598 convolutional units arranged in a specific sequence (Fig. S1). Each residual block
599 includes three hyper-parameters: N, W, and D. N represents the number of

convolutional kernels, W signifies the window size, and D indicates the dilation rate of each convolutional kernel. Given that a convolutional kernel with window size W and dilation rate D processes features across (W-1)×D neighboring positions, a residual block with two convolutional units can handle features across 2(W-1)×D neighboring positions. As a result, a TranslationAI model with K stacked residual blocks is capable of extracting features spanning $\sum_{i=1}^{K} 2(W_i - 1)D_i$ neighboring positions, where N_i, W_i, and D_i correspond to the hyper-parameters of the i-th residual block.

Model training and testing

To obtain a comprehensive, well-curated, and non-redundant set of sequences, we utilized the RefSeq gene annotation and extracted 47,098 protein-coding transcripts with 47,098 TIS-TTS pairs. Different splicing isoforms of the same gene are treated as different transcripts. For model training, we selected transcripts located on chromosomes 2, 4, 6, 8, 10-22, X, and Y, which contain 13,707 genes with 34,292 TIS-TTS pairs. For model evaluation, the transcripts from chromosomes 1, 3, 5, 7, and 9, containing 5,524 genes with 12,806 TIS-TTS pairs, were used. To mitigate overfitting, 10% of the training set were randomly chosen for early-stopping determination during training, while the remainder were used for model training.

We employed a sequence-to-sequence approach with a chunk size of 6,000 for model training and testing. The full-length mature mRNA sequences were one-hot encoded, with A, C, G, and U mapped to [1, 0, 0, 0], [0, 1, 0, 0], [0, 0, 1, 0], and [0, 0,

0, 1], respectively. We then zero-padded the one-hot encoded nucleotide sequences until their lengths were multiples of 6,000 and further padded them with flanking sequences of length S/2 at the beginning and end, where S corresponds to 60, 200, 600, or 2,000 for the TranslationAI-60, TranslationAI-200, TranslationAI-600, and TranslationAI-2k models, respectively. The padded nucleotide sequences were divided into blocks of length S/2 + 6,000 + S/2, with the i-th block consisting of nucleotide positions from 6,000(i-1) – S/2 + 1 to 6,000i + S/2. In parallel, the output label sequences were one-hot encoded as TIS ([0, 1, 0]), TTS ([0, 0, 1]), or neither ([1, 0, 0]). The one-hot encoded TIS/TTS output label sequences were also zero-padded until their lengths reached multiples of 6,000, and then split into 6,000-length blocks, with the i-th block containing positions from 6,000(i-1) + 1 to 6,000i. These one-hot encoded nucleotide sequences and their corresponding label sequences served as the inputs and outputs for the models, respectively.

The models were trained for 10 epochs using a batch size of 18 on two NVIDIA Tesla K80 GPUs. During training, the categorical cross-entropy loss between target and predicted outputs was minimized using the Adam optimizer. The optimizer's learning rate was set to 0.001 for the first six epochs and halved in each subsequent epoch. For each model, the training procedure was repeated 10 times, and the top five models based on performance were selected. During testing, each input was assessed using all five trained models, and the average of their outputs was utilized as the predicted output. This rigorous training and testing process aimed to ensure optimal performance and reliability in the resulting models.

The performance of the TIS/TTS prediction models was measured with top-k accuracy. This metric measures the fraction of correctly predicted positions among the top-k predicted sites, where k represents the number of true TIS/TTS sites in the dataset. For example, if the dataset contains k1 TISs and k2 TTSs, we set the score cutoff to predict exactly the top-k1 and top-k2 positions as TIS and TTS sites, respectively. It is worth noting that, unless specifically mentioned otherwise, only the top-k predicted sites were used for downstream analysis in our study.

During the development of the model, we have experimented with various hyper-parameters of this mode, including the input window size (60 nt, 200 nt, 600 nt, 2k and even 10k) and different convolutional filter sizes. However, it is worth noting that we did not systematically tune the model hyper-parameters. Therefore, the model hyper-parameters used here may not represent the optimal combinations. The results shown in the study probably represent the lower bound of this deep learning framework in the task of predicting TIS and TTS.

Role of transcript lengths in mRNA translation

To study the effect of transcript length on translation sites prediction, we sorted the mRNAs in order of increasing length. Using the TranslationAI-200 and TranslationAI-2k models, we calculated the positive rate of TIS/TTS for each transcript by comparing the number of positive TISs to the total number of transcripts with lengths shorter than the given transcript. We plotted these positive rates against the transcript length, as shown in Fig. 1C. Additionally, we included a histogram of

transcript lengths from the 47,098 transcripts analyzed in the background of the figure.

Perturbations of synonymous mutation

To investigate the impact of codon bias on predictions, we introduced perturbations by substituting codons with synonymous counterparts. Three scenarios were considered: 1) Random Synonymous Substitutions: Codons were randomly replaced with synonymous counterparts. 2) Higher CAI Substitutions: Codons were replaced with synonymous counterparts possessing a higher CAI. The Relative Synonymous Codon Usage (RSCU) for each codon was obtained from the Codon Statistics Database (http://codonstatsdb.unr.edu). The RSCU values were calculated based on genes encoding ribosomal proteins, known for their high expression and consequent strong codon bias (40). 3) Lower CAI Substitutions: Codons were replaced with synonymous counterparts possessing a lower CAI, following the same procedure as described above.

Occlusion sensitivity analysis

To assess the feature importance of individual positions in predicting TIS and TTS, we performed the occlusion sensitivity analysis, which provides a clear visualization of the contribution of each nucleotide to the scoring of TIS and TTS in an mRNA sequence. We masked each nucleotide in the mRNA with “N” one by one, and calculated the resulting score change of the predicted TIS/TTS.

688

689 **Codon distribution at upstream of stop codon**

690 To examine the codon distribution upstream of stop codon, we quantified the
691 frequency of each codon at the -30nt position relative to both strong and weak stop
692 codons. Specifically, we calculated the frequency of each codon as the number of
693 occurrences of that codon at the -30nt position divided by the total number of RNAs
694 analyzed at that position.

695

696 **Conservation analysis**

697 To evaluate the conservation levels of different RNAs, we obtained the
698 PhastCons46 scores from the PhastCons46 or PhyloP46 track in the UCSC Genome
699 Browser. These scores were generated from genome alignments of 46 vertebrates,
700 including human (hg19), and provide a measure of evolutionary conservation across
701 species. Each box plot displays the median as the central line, while the upper and
702 lower edges of the box represent the first and third quartiles, respectively.

703

704 **Non-canonical TISs/TTSs identification**

705 To systematically identify non-canonical TISs and TTSs in transcriptomes, we
706 input human transcriptome into TranslationAI model and retained only those RNAs
707 that met the threshold criteria (prediction score > 0.5) for both TIS and TTS as
708 translatable RNAs. The ncRNA dataset were retrieved from Ensembl build 75, which
709 was previously used in the published study (8) that identified hundreds of

710 noncanonical ORFs using ribosome profiling and mass-spectrometry.

711 To compare the TISs predicted by TranslationAI with TISs identified by ribosome
712 profiling, we expanded our predicted TIS library by retaining the top 10 TISs for each
713 gene predicted by the TranslationAI. This approach was necessary as ribosome
714 profiling often identifies multiple ORFs from one gene.

715 The alternative TISs were defined as the TIS with the highest score (>0.1),
716 excluding the annotated TIS. In addition, in-frame alternative TISs were defined as
717 TISs where the distance between the annotated TIS and alternative TIS is a multiple
718 of three.

719

720 **Ribosome footprint data analysis**

721 The ribosome profiling data analysis was performed on a previously published
722 ribosome footprint data that were retrieved from no drug treatment iPSC and iPSC-
723 induced iPSC-derived cardiomyocytes cells being deposited in GEO database under
724 accession number GSE131650. The genome assembly used throughout this
725 manuscript is hg19/GRCh37 annotated by GENCODE v27. We first filtered out reads
726 aligning to rRNAs using Bowtie v1.0.0 and aligned the remaining reads to the
727 annotated transcriptome with STAR v2.7.5a, using the --outSJfilterReads Unique --
728 outFilterMultimapNmax 1 --outFilterMismatchNmax 999 --
729 outFilterMismatchNoverReadLmax 0.04 to filter multiple aligned and redundant
730 reads. These alignments were assigned a specific P-site nucleotide using a 12-nt offset
731 from the 3′ end of reads. Metagene plots were generated by normalizing read density

732 around the start and stop codons of each gene (i.e, read depth at each position divided
733 by the average reads of each position in one transcript and the number of the covered
734 transcripts).
735 To estimate the correlation between predicted TIS/TTS scores and mRNA
736 translation efficiency, we ranked and divided the scores into percentiles (n~1580
737 transcripts/percentile, Fig. S2G-S2H). We calculated the translation efficiency of
738 transcripts from ribosome profiling data in two human cell lines as the ratio of Ribo-
739 seq read density to RNA-seq read density.
740

741 **Motif identification of strong and weak TISs/TTSs**

742 Motif discovery and analysis were performed using the Meme suite (v5.0.5). The
743 strong and weak TIS/TTS containing sequences (-30nt : + 33nt) were collected as
744 primary sequences for motif prediction. Additionally, all TIS/TTS containing
745 sequences (-30nt : +33nt) were used as control sequences. Meme was employed to
746 identify enriched motifs, with a maximum length of 63nt, that occur any number of
747 times within the given sequence.
748

749 **MS Proteomics and HLA Peptidomics data analysis**

750 MS-based proteomics data are deposited to the ProteomeXchange Consortium via
751 the Proteomics Identifications Database (PRIDE) partner repository with the dataset
752 identifier PXD014031 and PXD000394. Using an open search engine pFind (v3.1.3),
753 we searched the two previously published human proteome datasets against a combined

754 database (25692 proteins) containing all UniProt human proteins and the potential non-
755 canonical ORFs-coded peptides (uORFs, dORFs, dual frame ORFs, and new ORFs).
756 We selected positive mass spectra using following thresholds: $q < 0.01$, peptides length
757 $\geqslant 8$, missed cleavage sites $\leqslant 3$, allowing only common modifications (cysteine
758 carbamidomethylation, oxidation of methionine, protein N-terminal acetylation, pyro-
759 glutamate formation from glutamine, and phosphorylation of serine, threonine, and
760 tyrosine residues).

761 The resulting peptides were searched against non-redundant human protein
762 database using blastp-short and the peptides with less than two mismatches from known
763 proteins were removed.

764

765 **Transcriptomes of other species**

766 The genome sequence and gene annotations of *Mus musculus* (mm10), *Danio*
767 *rerio* (danRer11), *Drosophila melanogaster* (dm6), Ebola virus (eboVir3), SARS-
768 CoV-2 (wuhCor1), and human mitochondrion are obtained from UCSC database. The
769 sub-genomic sequences of SARS-CoV2 were obtained from a published study (36).
770 The genome sequence and gene annotation of Arabidopsis thaliana (TAIR10) are
771 obtained from TAIR database. Regarding E. coli (Escherichia coli K-12 substr.
772 MG1655), its transcription unit is retrieved from EcoCyc. The mRNA information (5′-
773 UTR, CDS, and 3′-UTR) for yeast was obtained from *Saccharomyces* Genome
774 Database (SGD). The genome sequence and gene annotation of Chloroplast
775 (Arabidopsis thaliana) was obtained from NCBI database. The genome sequence of

human mitochondria was obtained from NCBI database and its gene annotation file was obtained from GENCODE database.

Model comparison

TITER(20) (Translation Initiation siTE detectoR) is a deep learning-based framework designed to predict noncanonical TISs by incorporating both AUG and near-cognate start codons using high-throughput sequencing data. With the input of each TIS with its 200 nt flanking nucleotides, TITER outputs the probability of translation initiation for the given sequence. The source code for TITER was downloaded from https://github.com/zhangsaithu/titer. The TIS-predictor(23) is a machine learning model that was trained on instances of AUG and near-cognate start codon. The algorithm examines each codon and its 20 flanking nucleotides (23 nucleotides in total) to simulate and compute its probability score as a translation initiation site. The source code for TIS-predictor was downloaded from https://github.com/Agleason1/TIS-Predictor.

To evaluate the performance of TITER, TIS-predictor, and TranslationAI on canonical TIS AUG, we calculated the AUC, PR-AUC, and accuracy. For each RNA sequence input, we computed the probability score for all AUG codons, predicting the AUG with the highest score as the translation initiation site for each mRNA. These tools were tested on datasets from multiple species, including a Human test dataset and the whole transcriptomes of Mouse, Zebrafish, Drosophila, Arabidopsis, and the budding yeast (*S. cerevisiae*).

798

799 **Plasmid construction and Transfection**

800 To construct the reporter (pcDNA5-HA-GFP-stop_motif-Nluc-Flag) for testing
801 the translation readthrough products, the Fluc-Nluc luciferase sequence (a gift from
802 prof. Rachel Green) was cloned into pcDNA5 backbone digested by SpeI and XbaI
803 (41). The GFP sequence was amplified (fused with two BsmBI restriction fragments)
804 and inserted before Nluc. The modified VDR sequences were synthesized
805 (GENEWIZ) and cloned into BsmBI digested vector.

806 HEK293T cell line was cultured in DMEM (high glucose) medium containing
807 10% fetal bovine serum (FBS, Hyclone). To transient transfect plasmids into cells,
808 2 μg of reporters were transfected into cells in 6 well plate using lipofectamine 3000
809 (Invitrogen) according to the manufacturer's instruction. After 48 h, cells were
810 collected for further analysis of protein level.

811

812 **Western blot**

813 Cells were lysed in laemmli buffer, and the total cell lysates were resolved with 4-
814 20% ExpressPlus™ PAGE Gel (GeneScript). The following antibodies were used:
815 HA-Tag antibody (CST: 3724S) was diluted by 1:2000, V5 antibody (CST: 13202S)
816 was diluted by 1:2000, Flag antibody (Sigma: F1804-1MG) was diluted by 1:2000.
817 The HRP-linked secondary antibodies (CST: 7076S) were used by 1:4000 dilution
818 and the blots were visualized with the ECL reagents (Bio-Rad).

819

820 **Data and software availability**

Training and testing data, prediction scores for all possible single nucleotide substitutions in the reference genome and source code are publicly hosted at GitHub (https://github.com/rnasys/TranslationAI). Prediction scores and source code are publicly released under GPL v3 and are free for use for academic and non-commercial applications.

Acknowledgments

We thank Dr. Rachel Green for kindly sharing the plasmids of translation read-through and offering insightful suggestions on the potential mechanisms of translation termination. This work is supported by the Strategic Priority Research Program of Chinese Academy of Sciences (XDB38040100 to Z.W.), the National Key Research and Development Program of China (2021YFA1300503 and 2018YFA0107602 to Z.W.), the National Natural Science Foundation of China (32030064, 32250013, 91940303 and 31730110 to Z.W.; 32100430 to X.F.), the Starry Night Science Fund at Shanghai Institute for Advanced Study of Zhejiang University (SN-ZJU-SIAS-009) and the NIH Basic Research in Cancer Health Disparities Award to S.R.P. and J.A.F. (R01CA220314). Z.W. is also supported by CAS Interdisciplinary Innovation Team and the type A CAS Pioneer 100-Talent program.

Author Contributions

Conceptualization, Z.W., X.F. and T.C.; Methodology, X.F., T.C., and Z.W.; Software, X.F. and T.C.; Experiments, C.C.; Writing and discussion, X.F., Z.W., T.C.,

and M.H.; Funding acquisition, X.F., and Z.W.

Declaration of Interests

The authors declare no competing financial interests.

References

1. Frankish, A., Diekhans, M., Ferreira, A.M., Johnson, R., Jungreis, I., Loveland, J., Mudge, J.M., Sisu, C., Wright, J., Armstrong, J. *et al.* (2019) GENCODE reference annotation for the human and mouse genomes. *Nucleic Acids Res*, **47**, D766-D773.
2. Mouilleron, H., Delcourt, V. and Roucou, X. (2016) Death of a dogma: eukaryotic mRNAs can code for more than one protein. *Nucleic Acids Res*, **44**, 14-23.
3. Hinnebusch, A.G. (2011) Molecular mechanism of scanning and start codon selection in eukaryotes. *Microbiol Mol Biol Rev*, **75**, 434-467, first page of table of contents.
4. McNair, K., Ecale Zhou, C.L., Souza, B., Malfatti, S. and Edwards, R.A. (2021) Utilizing Amino Acid Composition and Entropy of Potential Open Reading Frames to Identify Protein-Coding Genes. *Microorganisms*, **9**.
5. Jackson, R., Kroehling, L., Khitun, A., Bailis, W., Jarret, A., York, A.G., Khan, O.M., Brewer, J.R., Skadow, M.H., Duizer, C. *et al.* (2018) The translation of non-canonical open reading frames controls mucosal immunity. *Nature*, **564**, 434-438.
6. Matsumoto, A., Pasut, A., Matsumoto, M., Yamashita, R., Fung, J., Monteleone, E., Saghatelian, A., Nakayama, K.I., Clohessy, J.G. and Pandolfi, P.P. (2017) mTORC1 and muscle regeneration are regulated by the LINC00961-encoded SPAR polypeptide. *Nature*, **541**, 228-232.
7. Yang, Y., Fan, X., Mao, M., Song, X., Wu, P., Zhang, Y., Jin, Y., Yang, Y., Chen, L.L., Wang, Y. *et al.* (2017) Extensive translation of circular RNAs driven by N(6)-methyladenosine. *Cell Res*, **27**, 626-641.
8. Chen, J., Brunner, A.D., Cogan, J.Z., Nunez, J.K., Fields, A.P., Adamson, B., Itzhak, D.N., Li, J.Y., Mann, M., Leonetti, M.D. *et al.* (2020) Pervasive functional translation of noncanonical human open reading frames. *Science*, **367**, 1140-1146.
9. Raj, A., Wang, S.H., Shim, H., Harpak, A., Li, Y.I., Engelmann, B., Stephens, M., Gilad, Y. and Pritchard, J.K. (2016) Thousands of novel translated open reading frames in humans inferred by ribosome footprint profiling. *Elife*, **5**.
10. Jaganathan, K., Kyriazopoulou Panagiotopoulou, S., McRae, J.F., Darbandi, S.F., Knowles, D., Li, Y.I., Kosmicki, J.A., Arbelaez, J., Cui, W., Schwartz, G.B. *et al.* (2019) Predicting Splicing from Primary Sequence with Deep Learning. *Cell*, **176**, 535-548 e524.
11. Jumper, J., Evans, R., Pritzel, A., Green, T., Figurnov, M., Ronneberger, O., Tunyasuvunakool, K., Bates, R., Zidek, A., Potapenko, A. *et al.* (2021) Highly accurate protein structure prediction with AlphaFold. *Nature*, **596**, 583-589.
12. Eraslan, G., Avsec, Z., Gagneur, J. and Theis, F.J. (2019) Deep learning: new computational modelling techniques for genomics. *Nat Rev Genet*, **20**, 389-403.
13. Bogard, N., Linder, J., Rosenberg, A.B. and Seelig, G. (2019) A Deep Neural Network for Predicting and Engineering Alternative Polyadenylation. *Cell*, **178**, 91-106 e123.
14. Zhou, J., Theesfeld, C.L., Yao, K., Chen, K.M., Wong, A.K. and Troyanskaya, O.G. (2018) Deep learning sequence-based ab initio prediction of variant effects on expression and disease risk. *Nat Genet*, **50**, 1171-1179.
15. Vamathevan, J., Clark, D., Czodrowski, P., Dunham, I., Ferran, E., Lee, G., Li, B., Madabhushi, A., Shah, P., Spitzer, M. *et al.* (2019) Applications of machine learning in drug discovery and development. *Nat Rev Drug Discov*, **18**, 463-477.

16. Sonenberg, N. and Hinnebusch, A.G. (2009) Regulation of translation initiation in eukaryotes: mechanisms and biological targets. *Cell*, **136**, 731-745.
17. Lee, S., Liu, B., Lee, S., Huang, S.X., Shen, B. and Qian, S.B. (2012) Global mapping of translation initiation sites in mammalian cells at single-nucleotide resolution. *Proc Natl Acad Sci U S A*, **109**, E2424-2432.
18. Gao, X., Wan, J., Liu, B., Ma, M., Shen, B. and Qian, S.B. (2015) Quantitative profiling of initiating ribosomes in vivo. *Nat Methods*, **12**, 147-153.
19. Chen, W., Feng, P.M., Deng, E.Z., Lin, H. and Chou, K.C. (2014) iTIS-PseTNC: a sequence-based predictor for identifying translation initiation site in human genes using pseudo trinucleotide composition. *Anal Biochem*, **462**, 76-83.
20. Zhang, S., Hu, H., Jiang, T., Zhang, L. and Zeng, J. (2017) TITER: predicting translation initiation sites by deep learning. *Bioinformatics*, **33**, i234-i242.
21. Goel, N., Singh, S. and Aseri, T.C. (2020) Global sequence features based translation initiation site prediction in human genomic sequences. *Heliyon*, **6**, e04825.
22. Kalkatawi, M., Magana-Mora, A., Jankovic, B. and Bajic, V.B. (2019) DeepGSR: an optimized deep-learning structure for the recognition of genomic signals and regions. *Bioinformatics*, **35**, 1125-1132.
23. Gleason, A.C., Ghadge, G., Chen, J., Sonobe, Y. and Roos, R.P. (2022) Machine learning predicts translation initiation sites in neurologic diseases with nucleotide repeat expansions. *PLoS One*, **17**, e0256411.
24. Leppek, K., Das, R. and Barna, M. (2018) Functional 5' UTR mRNA structures in eukaryotic translation regulation and how to find them. *Nat Rev Mol Cell Biol*, **19**, 158-174.
25. Mayr, C. (2019) What Are 3' UTRs Doing? *Cold Spring Harb Perspect Biol*, **11**.
26. Fields, A.P., Rodriguez, E.H., Jovanovic, M., Stern-Ginossar, N., Haas, B.J., Mertins, P., Raychowdhury, R., Hacohen, N., Carr, S.A., Ingolia, N.T. *et al.* (2015) A Regression-Based Analysis of Ribosome-Profiling Data Reveals a Conserved Complexity to Mammalian Translation. *Mol Cell*, **60**, 816-827.
27. Kozak, M. (1987) An analysis of 5'-noncoding sequences from 699 vertebrate messenger RNAs. *Nucleic Acids Res*, **15**, 8125-8148.
28. Kozak, M. (1986) Point mutations define a sequence flanking the AUG initiator codon that modulates translation by eukaryotic ribosomes. *Cell*, **44**, 283-292.
29. Loughran, G., Jungreis, I., Tzani, I., Power, M., Dmitriev, R.I., Ivanov, I.P., Kellis, M. and Atkins, J.F. (2018) Stop codon readthrough generates a C-terminally extended variant of the human vitamin D receptor with reduced calcitriol response. *J Biol Chem*, **293**, 4434-4444.
30. Mills, E.W., Wangen, J., Green, R. and Ingolia, N.T. (2016) Dynamic Regulation of a Ribosome Rescue Pathway in Erythroid Cells and Platelets. *Cell Rep*, **17**, 1-10.
31. de Klerk, E. and t Hoen, P.A. (2015) Alternative mRNA transcription, processing, and translation: insights from RNA sequencing. *Trends Genet*, **31**, 128-139.
32. Manske, F., Ogoniak, L., Jurgens, L., Grundmann, N., Makalowski, W. and Wethmar, K. (2023) The new uORFdb: integrating literature, sequence, and variation data in a central hub for uORF research. *Nucleic Acids Res*, **51**, D328-D336.
33. Wan, J. and Qian, S.B. (2014) TISdb: a database for alternative translation initiation in mammalian cells. *Nucleic Acids Res*, **42**, D845-850.
34. Huang, J.Z., Chen, M., Chen, D., Gao, X.C., Zhu, S., Huang, H., Hu, M., Zhu, H. and Yan,

G.R. (2017) A Peptide Encoded by a Putative lncRNA HOXB-AS3 Suppresses Colon Cancer Growth. *Mol Cell*, **68**, 171-184 e176.

35. Stern-Ginossar, N., Thompson, S.R., Mathews, M.B. and Mohr, I. (2019) Translational Control in Virus-Infected Cells. *Cold Spring Harb Perspect Biol*, **11**.

36. Wang, D., Jiang, A., Feng, J., Li, G., Guo, D., Sajid, M., Wu, K., Zhang, Q., Ponty, Y., Will, S. *et al.* (2021) The SARS-CoV-2 subgenome landscape and its novel regulatory features. *Mol Cell*, **81**, 2135-2147 e2135.

37. Banerjee, A.K., Blanco, M.R., Bruce, E.A., Honson, D.D., Chen, L.M., Chow, A., Bhat, P., Ollikainen, N., Quinodoz, S.A., Loney, C. *et al.* (2020) SARS-CoV-2 Disrupts Splicing, Translation, and Protein Trafficking to Suppress Host Defenses. *Cell*, **183**, 1325-1339 e1321.

38. Tunney, R., McGlincy, N.J., Graham, M.E., Naddaf, N., Pachter, L. and Lareau, L.F. (2018) Accurate design of translational output by a neural network model of ribosome distribution. *Nat Struct Mol Biol*, **25**, 577-582.

39. He, K., Zhang, X., Ren, S. and Sun, J. (2016) Deep Residual Learning for Image Recognition. *Proceedings of the IEEE Conference on Computer Vision and Pattern Recognition*, 770-778.

40. Subramanian, K., Payne, B., Feyertag, F. and Alvarez-Ponce, D. (2022) The Codon Statistics Database: A Database of Codon Usage Bias. *Mol Biol Evol*, **39**.

41. Wangen, J.R. and Green, R. (2020) Stop codon context influences genome-wide stimulation of termination codon readthrough by aminoglycosides. *Elife*, **9**.

Figures and legends

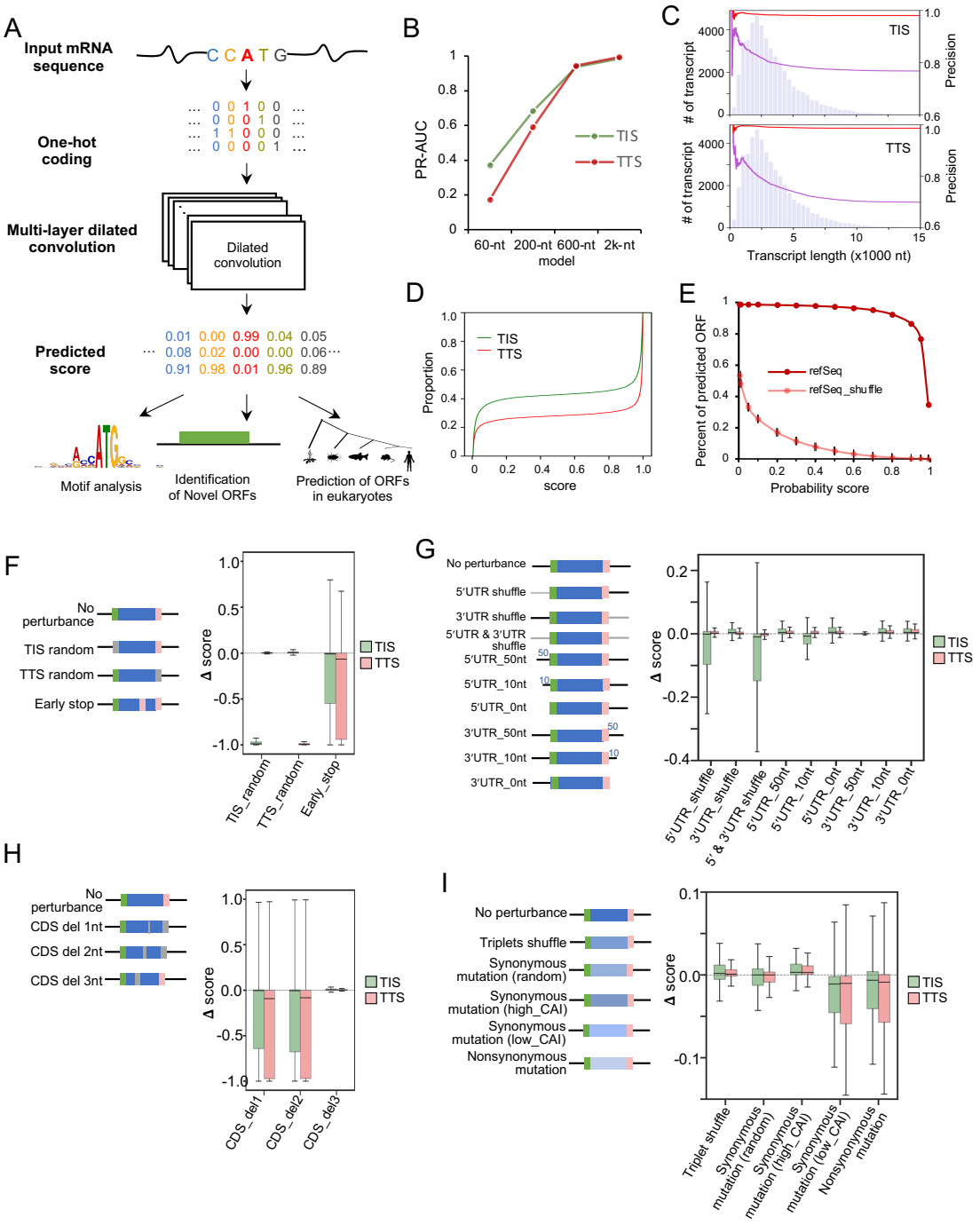

Figure 1. Construction of deep learning network for translation prediction. A. Flowchart of TranslationAI, a computational model for predicting translation initiation and termination sites with full length mRNA. For each position in the full length mRNA, TranslationAI-2k takes 60, 200, 600, and 2,000 nucleotides of flanking sequence as input, and predicts whether that position corresponds to a translation initiation site (TIS), translation termination site (TTS), or neither. **B.** Effect of input sequence context size

on network accuracy. PR-AUC is the area under the precision-recall curve. The figure shows the performance of the network at four different input sequence context sizes. **C.** Relationship between transcript length and the positive rate of TIS/TTS for each transcript by comparing the number of positive TISs from TranslationAI-200 (purple line) or TranslationAI-2k (red line) to the total number of transcripts with lengths shorter than the given transcript. The distribution of transcript length is shown in the background as a histogram. **D.** Accumulative distribution of TIS/TTS score among all mRNAs. **E**. The number of ORFs predicted by TranslationAI-2k using mRNA and shuffled mRNA (mononucleotide shuffling) as input and different cutoff of TIS scores. The average number of ORFs predicted from multiple shuffling, along with error bars representing three times the standard deviation calculated from shuffled sequences. **F-I.** The features learned by TranslationAI. Systematic *in silico* perturbations on different regions of the mRNA, measured as changes (**Δ** score) in probability scores for the authentic TISs/TTSs. The perturbations include: **F**, replacement of TIS/TTS identity; **G**, changes in UTR length and sequence; **H**, frameshifts by deleting one, two, or three nucleotides; **I**, mutations in coding sequences. Blue box: ORF (open reading frame), black line: 5′-UTR and 3′-UTR, green line: TIS, pink line: TTS. Mononucleotide shuffling was performed for shuffling of 5′-UTR and 3′-UTR. Codon shuffling was performed for triplet shuffle, which maintained the amino acid composition. CAI: Codon Adaptation Index.

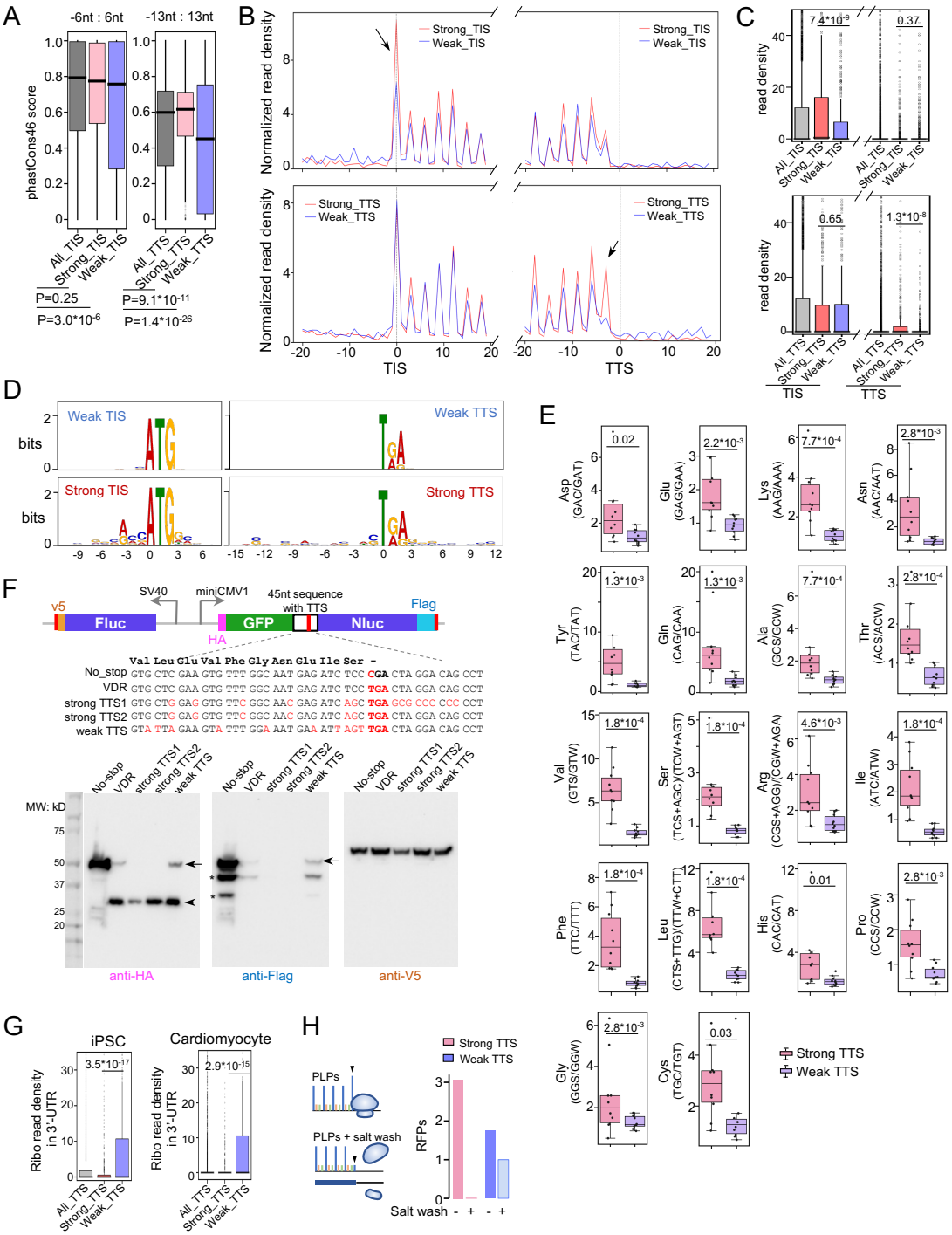

Figure 2. Evaluation of predictive features in TranslationAI. A. Conservation analysis of all TIS/TTS, strong TIS/TTS, and weak TIS/TTS regions. P-values were calculated using Mann–Whitney U test. **B.** Metagene analysis and **C.** boxplot of reads density on transcripts containing strong (red) and weak (blue) TIS/TTS (-20nt : +20nt) in iPSC cell line. P-values were calculated using Mann–Whitney U test. **D.** Motif analysis of strong and weak TIS/TTS. **E.** The codon distribution at the -30nt position

of stop codon. The ratios of the same amino acid with C/G and A/T at the third position of each codon before strong and weak stop codons was quantified. P-values were calculated using standard T-test. **F.** Validation of motifs around strong TTS. Known readthrough stop codon from VDR and their mutations (without change of amino acids) were tested for translation readthrough. No_stop: stop codon of VDR (TGA) was mutated to CGA; strong TTS1: stop codon of VDR was mutated to a strong TTS by changing the upstream 27nt and downstream 12nt sequences; strong TTS2: stop codon of VDR was mutated to a strong TTS by changing the upstream 27nt sequence; weak TTS: stop codon of VDR was mutated to a weak TTS by changing the upstream 27nt. See supplementary information in Table S3. **G.** Boxplot analysis of reads density on 3′-UTRs from transcripts with strong/weak TTS in iPSC cell line and iPSC-induced Cardiomyocyte cell line, respectively. **H.** Normalized read density (by abundance of the transcript) at the last P-site before stop codon of in vitro platelet-like particles (PLP) and PLP treated with high salt.

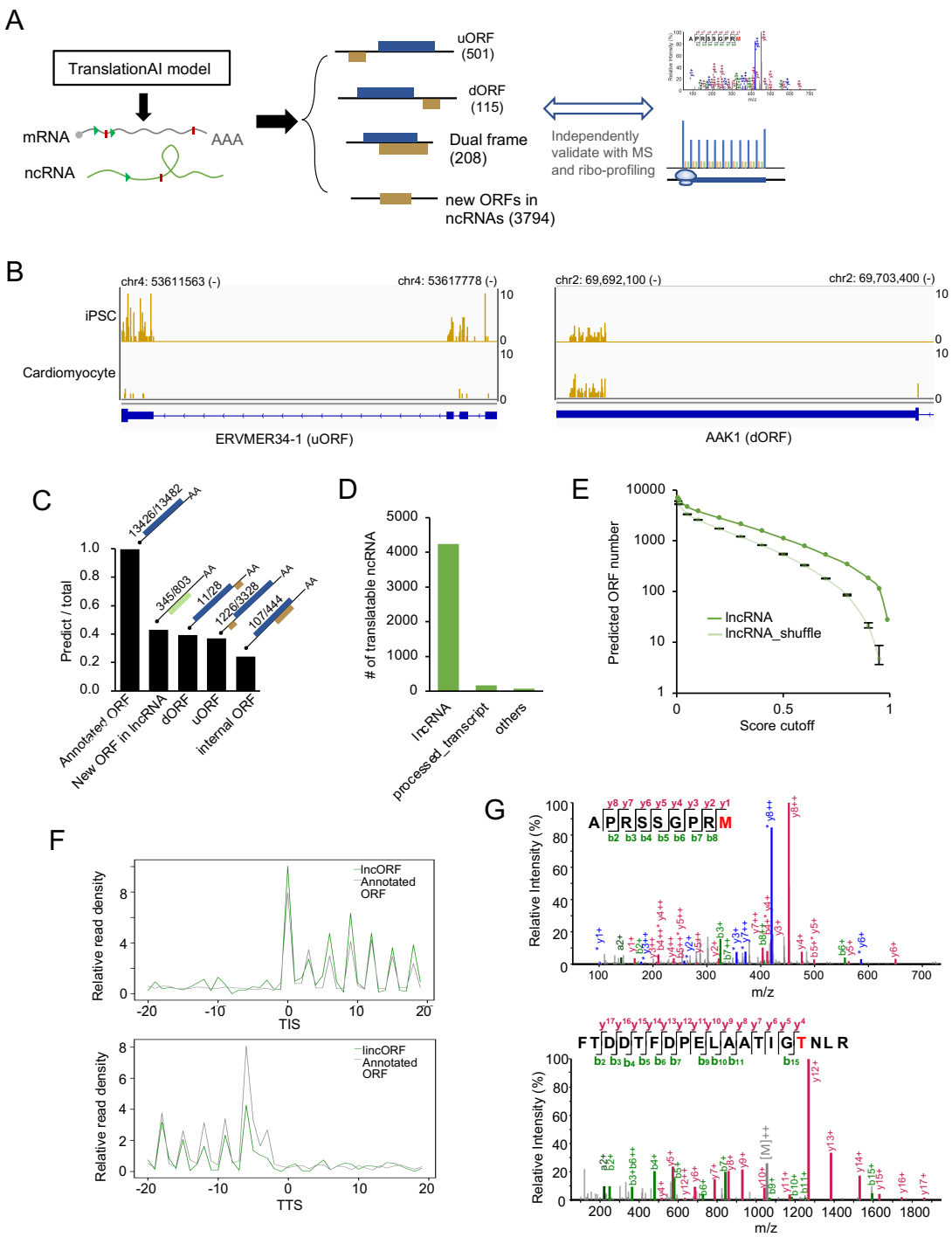

Figure 3. Identification of non-canonical ORFs in human transcriptome. A. Flowchart for identifying non-canonical ORFs, including upstream ORFs, downstream ORFs, dual coding ORFs, and new ORFs from non-coding RNAs. **B.** Example ribosome footprints of a uORF from ERVMER-1 and dORF from AAK1. **C.** The ratio of various types of predicted TISs identified by another published dataset derived from ribosome profiling assays. **D.** The number of newly identified translatable ncRNA in

annotated lncRNAs, processed transcripts and other transcripts without known ORFs. **E.** The number of ORFs predicted by TranslationAI-2k using non-coding RNA and shuffled non-coding RNA sequences as input. The average numbers of ORFs predicted from lncRNAs and shuffled lncRNAs (mononucleotide shuffling, as control) were shown, with error bars representing 3×standard deviation calculated from shuffled sequences. **F.** Metagene analysis of translatable lncRNAs (green line) and control (grey line, mRNAs with the same ORF length distribution of predicted ORFs from lncRNAs). **G.** The MS/MS spectra of peptides from two ncRNAs: lncRNA ENST00000609975 (APRSSGPRM) and antisense RNA ENST00000413405 (FTDDTFDPELAATIGTNLR). The annotated b- and y-ions are marked in red and green, respectively.

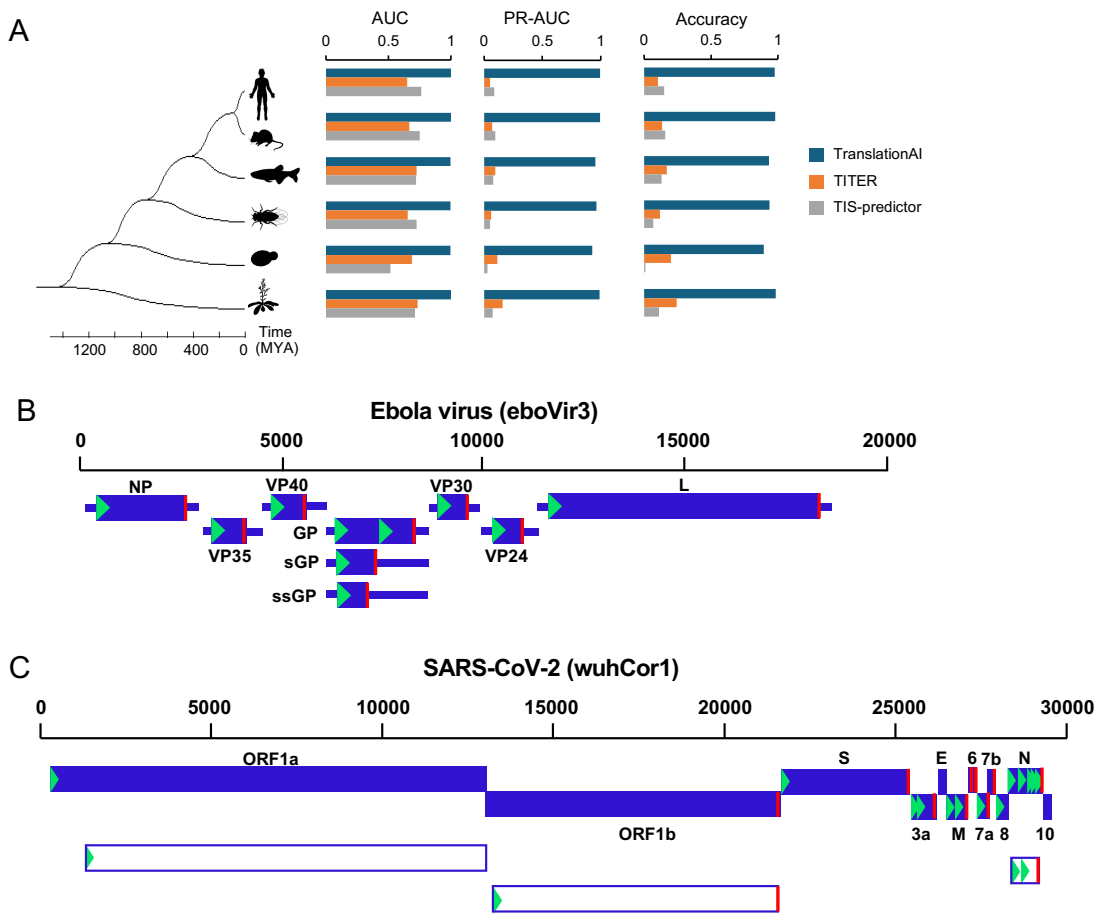

Figure 4. TranslationAI accurately predicts TIS/TTS of eukaryotes, prokaryotes, and viruses. A. The AUC, PR-AUC, and prediction accuracy of TIS prediction across tested eukaryotes (Human, Mouse, Zebrafish, Drosophila, Arabidopsis, and budding yeast *S. cerevisiae*). The predictions of two previous models are also included as a comparison. **B-C.** The prediction of TISs/TTSs on Ebola genomic or RNA sequences **B.** and SARS-CoV-2 genomic or subgenomic sequences **C.** The upper scales represent the genomic sequence position, the blue boxes indicate the annotated ORFs, and the white boxes indicate the newly predicted out-of-frame ORFs. The green triangles and red lines indicate the predicted in-frame TISs and TTSs, respectively.